In Situ Spectroscopic Observation of Activation and Transformation of Tantalum Suboxides

Ke Wang[1], Zhi Liu[2,3], Tirma Herranz Cruz[2], Miquel Salmeron[2,3], and Hong Liang[*1]

[1]Materials Science and Mechanical Engineering, Texas A&M University, College Station, Texas, 77843, USA

[2]Materials Sciences and Chemical Sciences Division, Lawrence Berkeley National Laboratory, Berkeley, CA 94720, USA

[3]Advanced Light Source, Lawrence Berkeley National Laboratory, Berkeley, CA 94720, USA

[*] Telephone : (979) 862-2623, Fax : (979) 845-3081, E-mail: hliang@tamu.edu

Abstract

Using ambient pressure X-ray Photoelectron Spectroscopy (AP-XPS), we were able to observe the process of oxidation of tantalum with different morphological parameters. Being able to trace surface evolution during oxidation, we evaluated activation energy of oxidation under the influence of strain and grain boundaries. It was found that the metal oxidized through three different stages and there was a transition stage where the phase transformation from suboxides to the equilibrium state of pentoxide. The applied stress and surface defects reduced the activation energy of oxidation.

[*] Corresponding Author: hliang@tamu.edu

Introduction

In light of advancement in high temperature oxide superconductors,[1] it has become increasingly important to understand the oxidation kinetics in all stages involved. Such a study however has been difficult for transition metals that possess several valence states involving multiple oxides. One of the key challenges in understanding metal oxidation is lack of high resolution and in situ observation techniques. In the past, in situ investigation was restricted due to the requirements of high vacuum.[2-4] Furthermore, oxidation is a dynamic process and observation of static conditions of a surface does not represent their real situations.[5,6] Recent development in ambient pressure X-ray photoelectron spectroscopy (AP-XPS) systems made it possible to study metal surfaces at near-ambient conditions.[7-9] The technique is beneficial to study materials with active electronic structures.

Metal oxidation has played important roles in fundamentals of materials and engineering applications.[10-14] Oxidation is either responsible for corrosion or for protection of the same in the form of a passivation layer.[11,15-18] It has been accepted that a metal oxidation process involves interactions of metals and oxygen on the surface. Such a process involves the chemisorption, surface oxidation, subsurface incorporation, and bulk oxidation.[11,19-23] The types of metal oxides and their relationships have not been well understood.

Tantalum (Ta) is a noble metal that is known to have an equilibrium state of pentoxide. Studies have reported that non-equilibrium state of Ta oxides could exist.[24,25] Discrete state of Ta oxide was found at elevated temperatures with a shift of 4f core level photoelectron spectra.[26] Continued oxygen exposure at low temperature led to oxidation of Ta.[27,28] Such oxidation began on the surface and then bulk through an electric-field-assisted diffusion mechanism. Most previous studies have been based on thermal effects. In present research, we investigate oxidation mechanisms of Ta under various mechanical and thermal conditions. The Ta has five valence states. We propose a non-conventional approach to study tantalum oxidation through mechanical stimulation. Using the AP-XPS technique, we are able to observe the initiation and growth of oxides on Ta of different surface morphological conditions. The activation energy of oxidation was evaluated based on such conditions.

Experimental

In present research, we conducted *in situ* high-resolution AP-XPS analysis of the oxidation process of polycrystal and single crystal (100) Ta. Subsurface incorporation and the kinetics of the oxidation were studied under oxygen pressure up to 0.1 Torr.

Sample preparation: Single crystal (100) (99.99%) and polycrystal Ta (99.9%) (Goodfellow) were used for this research. The polycrystal Ta contains crystal planes of (110), (200), (211), and (220). The polycrystal samples were divided into two sets. One set was compressed and the other as received. The compressed samples were prepared by

pressing the set of samples under a high pressure of about 16 GPa using the Instron Tensile Tester (Instron 4206).

An optical microscope (Polaroid DMC2) with polarized lens was used to characterize the grain boundary of test samples. Topographic and phase images at a small scale were obtained using an Atomic Force Microscope (Nano-R, Pacific Nanotechnology Inc.) in the close contact mode.

The AP-XPS measurements were carried out at the beamline 9.3.2 of the Advanced Light Source (ALS) at the Lawrence Berkeley National Laboratory. The beamline is equipped with a fixed angle 55m spherical grating monochromater and the Physical Electronics hemispherical analyzer.[29] The photoemission system was developed to operate at near-ambient pressures (up to 1 Torr) and the sample can be heated up to 700 K. Clean sample surfaces were prepared by Ar^+ sputtering (2 keV) for 2 hrs in the preparation chamber, then transferred to the ambient pressure chamber for spectra acquisition at the room temperature (RT) and 500 K under 0.1 torr of oxygen. Experiments were designed to imitate the real oxidation process because that any high-temperature oxidation starts with RT oxidation. The Ta 4f (hv = 550eV) and O 1s (hv = 850 eV) spectra were taken at the photon energy of 550eV and 850eV respectively to ensure the same electron kinetic energy, i.e., the identical depth information for all elements of interest. The dynamic oxidation process was recorded with a 50 s interval during the measurement. Different photoelectron energies were applied in order to obtain depth profiles of Ta 4f species. The photoelectron spectra were measured at normal-incidence geometry, and the binding energy (BE) was referenced to the Fermi edge. All spectra were normalized by the

corresponding energy-dependent X-ray photoionization cross sections.[30] Using XPSpeak 4.1, the peaks were deconvoluted with asymmetric Gauss-Lorentz profiles after the subtraction of a Shirley background.

Results

Figure 1 shows the Ta 4f and O 1s spectra of the as-received polycrystalline Ta under different oxidation conditions. Figures 1a, b, and c provide the spectra right after sputter cleaning (1a), after oxidation at room temperature (RT) (1b), and after oxidation at 500 K (1c). Further deconvolution identifies different valence states of Ta. From high to low binding energy (BE), they are Ta^{5+}, Ta^{3+}, Ta^{2+}, and mixture of Ta^{1+} and Ta^{0}. The deconvolution also presents the evolution of each component. With oxidation, the area ratio of Ta^{5+} increases and others decrease. Figure 1d compares the O 1s spectra of the sample under different conditions. Spectra after oxidation (at RT and 500 K) have higher intensity than that of the sample after sputter cleaning. They also have the same peak center at 530.2 eV. This number is smaller than that after sputter cleaning (530.4eV).

Figure 2 shows the Ta 4f and O 1s spectra of the compressed polycrystalline Ta under different oxidation conditions. Figures 2a, b, and c present the spectra of right after sputter cleaning, after oxidation at room temperature (RT), and after oxidation at 500 K, respectively. Spectrum deconvolution identifies all valence states of tantalum. From high to low binding energy (BE), they are Ta^{5+}, mixture of Ta^{4+} and Ta^{3+}, Ta^{2+}, and mixture of Ta^{1+} and Ta^{0}. The evolution of each component shows the same trend as in Figure 1. A comparison of the O 1s spectra is shown in Figure 2d. For polycrystal tantalum, the O 1s

spectra shift of the compressed sample is similar to that of the as-received. Spectra after oxidation (at RT and 500 K) have the same peak center at 530.2 eV. The peak center of that after sputter cleaning is at 530.6 eV.

Figure 3 shows the Ta 4f and O 1s spectra of the single crystalline tantalum under different oxidation conditions. Figures 3a, b, and c provide results that right after sputtering, after oxidation at room temperature (RT), and after oxidation at 500 K. Through deconvolution, the same six valence states are identified as shown in Figure 2 and their evolution trend behaves the same as polycrystalline tantalum samples. Figure 3d compares the O 1s spectra of the sample under different conditions. The peak center of the spectra after sputter cleaning and oxidation at the RT and 500 K are at 530.6 eV, 530.4 eV, and 530.2 eV, respectively. Results are different from that observed in the polycrystalline sample, which demonstrates the effects of crystal structure on the oxidation process.

For the as-received sample, the temporal evolution of Ta 4f spectrum is plotted in Figures 4a and b for oxidation at RT and 500 K. There is no sign of peak shift in the spectra of oxidation at RT. But for the oxidation at 500 K, a gradual shift toward higher BE can be identified. There are two possibilities for such a shift. One is the formation of suboxides and the other is due to the magnetic field induced by the heating current. It was confirmed by the deconvolution results that the former is responsible for the shift. The formation of the suboxides causing the peak shift was reported.[7]

For the compressed sample, Figures 4c and d plot the time evolution of Ta 4f spectrum for oxidation at RT and 500 K respectively. The gradual peak shift is observed in both cases. The difference is that the shift in oxidation at 500 K is more apparent than that in the as-received sample.

For the single crystalline sample, the temporal evolution of Ta 4f spectrum is plotted in Figures 4e and f for oxidation at RT and 500 K. The gradual peak shift toward high BE is confirmed in both cases. Comparing with the as-received and compressed samples, the single crystalline sample exhibited the largest shift amplitude.

Discussion

Oxidation Kinetics

The process of oxidation is discussed here. As shown in Figure 5a, the evolution of Ta^{5+} 4f during oxidation at room temperature follows a parabolic law. At 500 K, as shown in Figure 5b, there are three distinguishable stages: oxidation, transition, and stabilization. The oxidation stage is the formation of oxide. The transition stage is the phase transformation from suboxides to the pentoxide. This is seen as the ratio increase of the $Ta5^{+}$ in Figure 5. The stabilization is the final stage when the oxidation is stablized with majority Ta pentoxide. According to our results, the oxidation at 500k was dominated by the transition between tantalum suboxidies and pentoxide, which appeared to be promted by the temperature increase.

The initial oxidation at room temperature can be explained using the fraction of free surface area. Comparing to the single crystal tantalum, the polycrystalline Ta has larger surface area due to its grain boundaries and surface defects. These will supply sufficient active sites for oxygen to incorporate leading to subsequent oxidation. Similarly, the as-received and compressed samples exhibit steeper slope than the single crystal one with excessive surface areas and defects, as shown in Figure 5a. Similar parabolic behavior had been reported in copper oxidation. [31] Our results are consistent with previously published data.

Activation Energy of Tantalum Oxidation

The observed peak shifts in Figure 4 are plotted in Figures 6a, b, and c for as-received polycrystalline, compressed polycrystalline, and single crystalline, respectively. The results of as-received and compressed samples indicate the existence of two slopes. Differently from the as-received and compressed samples, the single crystalline exhibits a linear shift of the peak center toward the high energy direction. The peak shifts suggest alternate oxidation processes underwent in each sample.

Figure 5a shows the time evolution of Ta^{5+} 4f during oxidation at RT. The as-received, compressed, and single crystal samples exhibit different behaviors while the as-received and compressed samples present similar evolving trend. The single crystal sample gives a lower slope than the other two. A close inspection also reveals two steps at 2000 s and 4000 s.

The temporal evolution of Ta^{5+} 4f during oxidation at 500 K is provided in Figure 5b. Comparing that at RT, the oxidation process at 500 K underwent in a different manner. Three different oxidation stages (I-III) are observed. At the primary stage (I), the formation of tantalum pentoxide is slow. In the transition stage (II), the oxidation rate varies in three samples. The single crystal sample has the steepest gradient and ends up with the highest pentoxide ratio following by the as-received sample. The compressed sample has the slowest increase with the lowest pentoxide ratio. At the final stage (III), the formation of Ta pentoxide reached a plateau and the oxidation became stabilized. The curves indicate that there is a limiting value for each sample. For the single crystal sample, the curve had a limiting value of 82.5% within a period of 1500 s. For the as-received, the data had a limiting value of 78% in a period of 2500 s. For the compressed, the curve reached a limiting value of 76.5% within a period of 2500 s.

The observed results can be qualitatively explained by the Wanger model of oxidation. In the theory, the metal oxidation proceeds via the diffusion of metal ions through a neutral oxide layer, which is a rate limiting process.[32] The further oxidation of Ta to pentoxide is limited by the transportation of tantalum ions through the oxide film. Consequently, the oxidation process eventually will get stabilized.

The activation energies of these samples were calculated for the temperatures between 300 K (RT) and 500 K using the equation:

$$\ln(k) = -\frac{E_a}{R}\frac{1}{T}$$

here the T is absolute temperature (in Kelvin), K is reaction constant. The activation energy E_a can be obtained through evolution of Ta^{5+} 4f against temperature at the oxygen pressure of 0.1 Torr. Results are shown in the Figure 7. From a semilogarithmic plot of the oxidation rate of tantalum versus 1/T, the E_a was calculated to be ~ 59.7 kJ/mol (0.62 eV/atom) for the as-received polycrystalline sample, ~ 37.6 kJ/mol (0.39 eV/atom) for the compressed polycrystal, and ~ 115.3 kJ/mol (1.2 eV/atom) for the single crystal. The calculated value for single crystalline sample is in agreement with the reported value.[33]

Comparing the activation energy, it is noticed that the calculated value for the compressed sample is 0.23 eV, less than the as-received. We believe this can be due to the strain effect on the reactivity of metal surfaces. To address this issue, we used an optical microscope (OM) and an atomic force microscope (AFM), along with the AP-XPS to study the effects of surface morphological changes and stress on Ta oxidation.

During sample preparation, the tantalum foil was cut into small pieces with the dimension of 8.25 mm ×8.46 mm ×1.12mm. They are subsequently compressed under a 11,360 kg (25,000 Lb) load, i.e., in the pressure of 162.76×10^6 kg/cm^2 or ~16 GPa. Two heads of Instron (Model 4206) have larger area than the sample to avoid extra stress concentration. The high compressive stress is significant enough to induce plastic deformation. Indeed, after compression, the sample size was changed to the dimension of 8.31 mm ×9.25 mm ×1.01mm. The remaining stress inside the Ta was around 1.3 GPa, based on the simple estimation through the stress-strain relationship.

Our results (in Figure 5) showed that the pentoxide increases with time at a different rate for each specimen. The difference of single crystalline and the polycrystal is in grain boundaries. Figure 8 is the optical microscopic image of tested samples. The polycrystalline Ta has visible grain boundaries. The height difference between grains varies from 30 to 40 nm. The height variance of these grain boundaries seems to be reduced in the compressed sample. The surface defects, deformation, and dislocations are expected to be introduced due to severe compression. The phase image of the AFM shows three sample surfaces are relatively uniform indicating no extra phase exists. The AFM height image shows that the polycrystalline surface has a higher surface roughness value as compared with the single crystal one. This is due to the existence of grain boundaries. The compressed has a median roughness in comparison with others. Based the observation of surface morphology shown in Figure 8, the higher oxidation rate of the as-received sample at room temperature (Figure 5a) is due to the extra effects introduced through grain boundaries. At 500K, the as-received sample has a lower transition rate than the single crystal one. This indicates that the as-received sample has more suboxides than that of single crystal. The transition from suboxides to pentoxide seems to dominate the oxidation process.

It has been reported that strained metal surfaces represented different chemical properties comparing with unstrained ones. One of the strain effects is the vibrational frequency shift of chemisorpted gas molecules such as CO (on Cu). [34] The other is the position of chemisorption [35], where gas molecules prefer to stay at the position under a tensile stress and the compressed regions otherwise. [36] In our case, the oxidation process underwent

three stages: oxidation, transition, and stabilization. In the compressed sample, a 16 GPa pressure was applied onto the sample in Z direction and caused severe plastic deformation. The residual stress was mainly tensile on the surface and compressive in the Z direction. Based on previous studies, the compressive stress does not promote chemisorption of oxygen. This indicates that other factors such as diffusion and reaction might be dominants. The severally deformed Ta is expected to have tremendous amount of dislocations acting as hosting sites of chemisorption as well as diffusion paths. As a result, the oxidation took place with less energy barrier, in such, suboxides were formed easily. This can be seen clearly in the Figure 5b. The force-induced suboxides of Ta has been reported in our electro-chemical mechanical exerperiments.[24,25] As a matter of fact, the activation energy of the compressed sample is the lowest as compared with the other two, as listed in Table 1.

Conclusions

Using ambient pressure XPS, we have studied the oxidation kinetics of Ta (100) and polycrystalline samples. Our results demonstrate that there are three distinguishable stages: oxidation, transition, and stabilization. In the transition stage, there is a phase transformation from tantalum suboxides to pentoxide. The oxidation process at room temperature and 500 K exhibits quite different behaviors. At the room temperature, the transition state is dominant by the defects and grain boundaries. At 500 K, the oxidation stage is well pronounced followed by the transition. The transition was completed at around 1500 second and become stabilized. The corresponding activation energies of

oxidation were obtained. Our results confirmed the effect of residual stress at the sample surface.

Acknowledgements

This research was sponsored by the National Science Foundation (0535578). The Advanced Light Source is supported by the Director, Office of Science, Office of Basic Energy Sciences, of the U.S. Department of Energy under Contract No. DE-AC02-05CH11231.

References

(1) Ohtomo, A.; Hwang, H. Y. *Nature* **2004**, *427*, 423.
(2) Campbell, C. T. *Science* **2001**, *294*, 1471.
(3) M. S. Chen; D. Kumar; Yi, C. W.; Goodman, D. W. *Science* **2005**, *310*, 291.
(4) G. Zheng; Altman, E. I. *Surf. Sci.* **2000**, *462*, 151.
(5) Ceyer, S. T. *Science* **1990**, *249*, 133.
(6) Ceyer, S. T. *Acc. Chem. Res.* **2001**, *34*, 737.
(7) G. Ketteler; D. F. Ogletree; H. Bluhm; H. Liu; E. L. D. Hebenstreit; Salmeron, M. *J. Am. Chem. Soc.* **2005**, *127*, 18269.
(8) D. F. Ogletree; H. Bluhm; G. Levedev; C. S. Fadley; Z. Hussain; Salmeron, M. *Rev. Sci. Instrum.* **2002**, *73*, 3872.
(9) Salmeron, M.; Schlögl, R. *Surf. Sci. Rep.* **2008**, *63*, 169.
(10) Over, H.; Seitsonen, A. P. *Science* **2002**, *297*, 2003.
(11) Over, H.; Kim, Y. D.; Seitsonen, A. P.; Wendt, S.; Lundgren, E.; Schmid, M.; Varga, P.; Morgante, A.; Ertl, G. *Science* **2000**, *287*, 1474.
(12) Thurmer, K.; Williams, E.; Reutt-Robey, J. *Science* **2002**, *297*, 2033.
(13) Kresse, G.; Schmid, M.; Napetschnig, E.; Shishkin, M.; Kohler, L.; Varga, P. *Science* **2005**, *308*, 1440.
(14) Nolte, P.; Stierle, A.; Jin-Phillipp, N. Y.; Kasper, N.; Schulli, T. U.; Dosch, H. *Science* **2008**, *321*, 1654.

(15) Hendriksen, B. L. M.; Frenken, J. W. M. *Phys. Rev. Lett.* **2002**, *89*, 046101.
(16) H. Demiryont; J. R. Sites; Geib, K. *Appl. Opt.* **1985**, *24*, 490.
(17) Chaneliere, C.; Autran, J. L.; Devine, R. A. B.; Balland, B. *Mat. Sci. Eng. R* **1998**, *22*, 269.
(18) P.M. Natishan; E. McCafferty; P.R. Puckett; Michel, S. *Corros. Sci.* **1996**, *38*, 1043.
(19) Gustafson, J.; Mikkelsen, A.; Borg, M.; Lundgren, E.; Köhler, L.; Kresse, G.; Schmid, M.; Varga, P.; Yuhara, J.; Torrelles, X.; Quirós, C.; Andersen, J. N. *Phys. Rev. Lett.* **2004**, *92*, 126102.
(20) Lundgren, E.; Gustafson, J.; Mikkelsen, A.; Andersen, J. N.; Stierle, A.; Dosch, H.; Todorova, M.; Rogal, J.; Reuter, K.; Scheffler, M. *Phys. Rev. Lett.* **2004**, *92*, 046101.
(21) Carlisle, C. I.; King, D. A.; Bocquet, M. L.; Cerdá, J.; Sautet, P. *Phys. Rev. Lett.* **2000**, *84*, 3899.
(22) Lundgren, E.; Kresse, G.; Klein, C.; Borg, M.; Andersen, J. N.; De Santis, M.; Gauthier, Y.; Konvicka, C.; Schmid, M.; Varga, P. *Phys. Rev. Lett.* **2002**, *88*, 246103.
(23) Li, W.-X.; Stampfl, C.; Scheffler, M. *Phys. Rev. Lett.* **2003**, *90*, 256102.
(24) Kar, P.; Wang, K.; Liang, H. *Electrochimi. Acta* **2008**, *53*, 5084.
(25) Kar, P.; Wang, K.; Liang, H. *Electrochem. &Solid-State Lett.* **2008**, *11*, 13.
(26) Himpsel, F. J.; Morar, J. F.; McFeely, F. R.; Pollak, R. A.; Hollinger, G. *Phys. Rev. B* **1984**, *30*, 7236.
(27) Pan, X.-H.; Qiu, S. L.; Raaen, S.; Florit, M. I.; Shek, M. L.; Strongin, M. *Phys. Rev. B* **1987**, *35*, 3740.
(28) Jacobsen, F. M.; Raaen, S.; Ruckman, M. W.; Strongin, M. *Phys. Rev. B* **1995**, *52*, 11339.
(29) Z. Hussain; W. R. A. Huff; S. A. Kellar; E. J. Moler; P. A. Heimann; W. McKinney; H. A. Padmore; C. S. Fadlley; Shirley, D. A. *J. Electron. Spectrosc. Relat. Phenom.* **1996**, *80*, 401.
(30) J. J. Yeh; Lindau, I. *At. Data Nucl. Data Tables* **1985**, *32*, 1.
(31) F. Gronlnd; Moller, P. J. *Surf. Sci.* **1987**, *184*, 530.
(32) Wagner, C. *Atom Movements*; ASM: Cleveland, 1951.
(33) F. Degreve; Drowart, J. *Metallurgie* **1966**, *6*, 115.
(34) Kampshoff, E.; Hahn, E.; Kern, K. *Phys. Rev. Lett.* **1994**, *73*, 704.
(35) Gsell, M.; Jakob, P.; Menzel, D. *Science* **1998**, *280*, 717.
(36) Mavrikakis, M.; Hammer, B.; Nørskov, J. K. *Phys. Rev. Lett.* **1998**, *81*, 2819.

Figure and Table Legends

Figure 1. XPS results of as-received polycrystalline tantalum. (a) Ta 4f after sputtering; (b) Ta 4f after oxidation at room temperature (RT); (c) Ta 4f after oxidation at 500 K; (d) Comparison of O 1s XPS results.

Figure 2. XPS results of compressed polycrystalline tantalum. (a) Ta 4f after sputtering; (b) Ta 4f after oxidation at room temperature (RT); (c) Ta 4f after oxidation at 500 K; (d) Comparison of O 1s XPS results.

Figure 3. XPS results of single crystalline tantalum. (a) Ta 4f after sputtering; (b) Ta 4f after oxidation at room temperature (RT); (c) Ta 4f after oxidation at 500 K; (d) Comparison of O 1s XPS results.

Figure 4. Time evolution of Ta 4f region during oxidation in 0.1 Torr O_2. (a) Oxidation of as-received sample at RT; (b) Oxidation of as-received sample at 500 K; (c) Oxidation of compressed sample at RT; (d) Oxidation of compressed sample at 500 K; (e) Oxidation of single crystal sample at RT; (f) Oxidation of single crystal sample at 500 K.

Figure 5. Plot of the intensities of Ta^{5+} 4f normalized to the total Ta 4f area as a function of time for three samples. (a) Oxidation at RT; (b) Oxidation at 500 K.

Figure 6. Peak shifts of Ta $4f_{7/2}$ during oxidation at 500 K. (a) As-received sample; (b) Compressed sample; (c) Single crystal sample.

Figure 7. Activation energy calculation of three samples oxidized at 500 K.

Figure 8. OM and AFM images of Ta samples. (a) As-received Ta polycrystalline; (b) Compressed Ta polycrystalline; (c) Ta single crystal (100).

Table 1. Activation energy.

Table 1. Calculated Activation Energy

Samples	Activation Energy (kJ/mol)	Activation Energy (eV/atom)
As-received	59.7	0.62
Compressed	37.6	0.39
Single Crystal (100)	115.3	1.2

Table of Contents

In Situ Spectroscopic Observation of Activation and Transformation of Tantalum Suboxides

Ke Wang, Zhi Liu, Tirma Herranz Cruz, Miquel Salmeron, and Hong Liang*

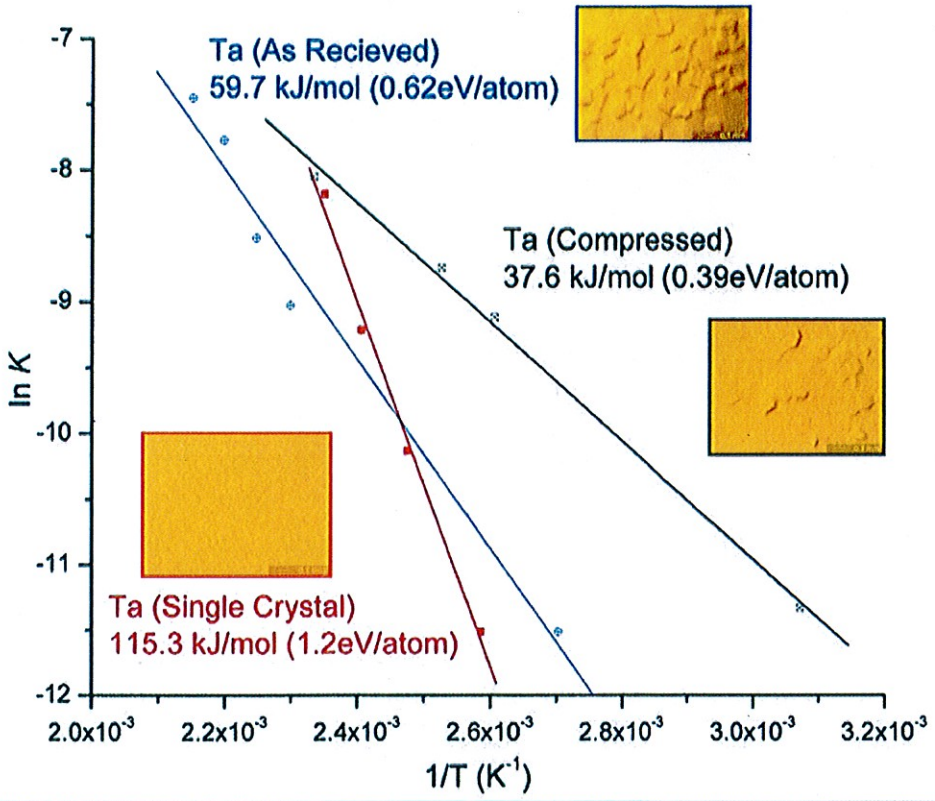

Abstract

Using ambient pressure X-ray Photoelectron Spectroscopy (AP-XPS), we were able to observe the process of oxidation of tantalum with different morphological parameters. Being able to trace surface evolution during oxidation, we evaluated activation energy of oxidation under the influence of strain and grain boundaries. It was found that the metal oxidized through three different stages and there was a transition stage where the phase transformation from suboxides to the equilibrium state of pentoxide. The applied stress and surface defects reduced the activation energy of oxidation.

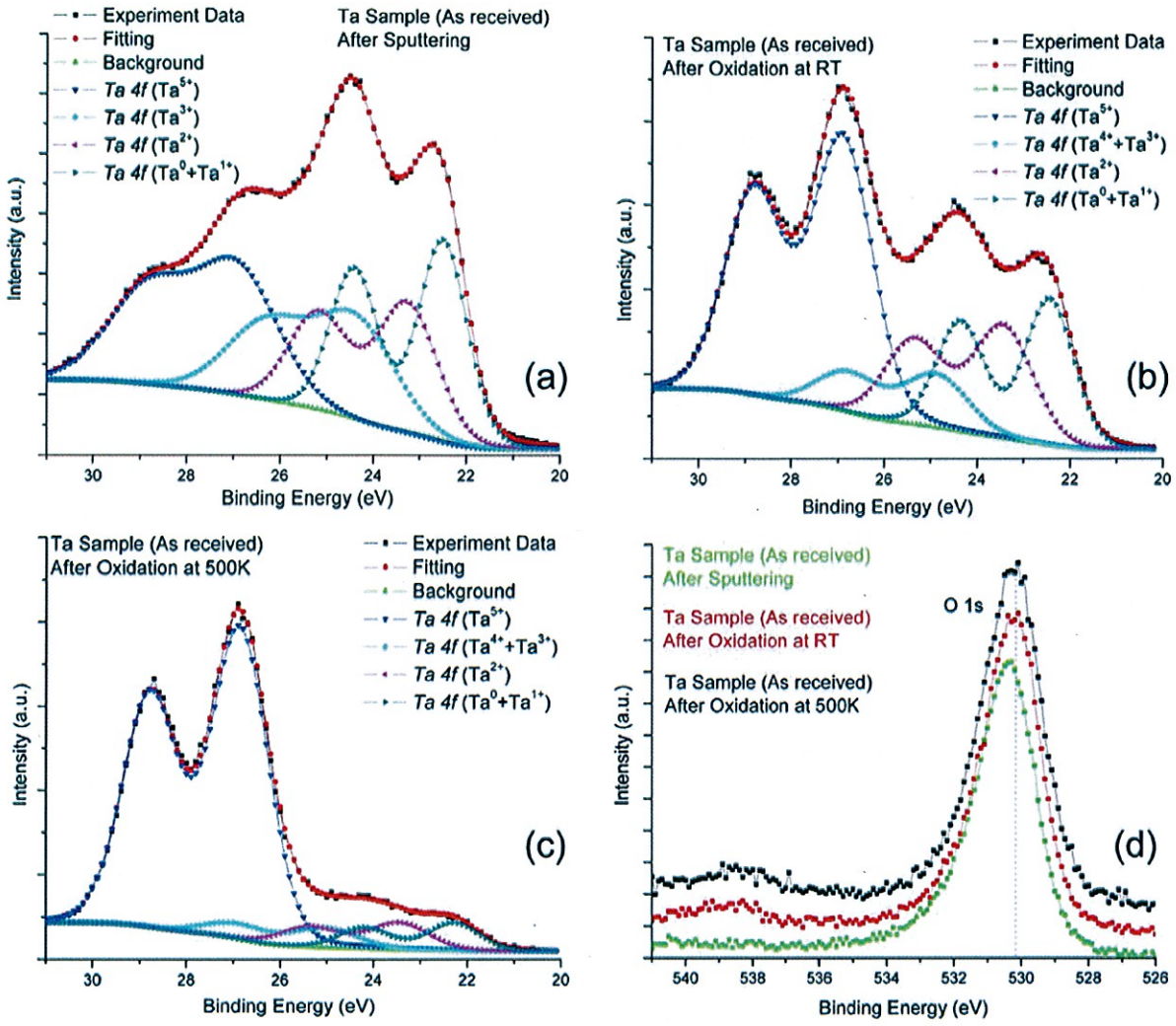

Figure 1. XPS results of as-received polycrystalline tantalum: (a) Ta 4f after sputtering; (b) Ta 4f after oxidation at RT; (c) Ta 4f after oxidation at 500 K; (d) comparison of O 1s XPS results.

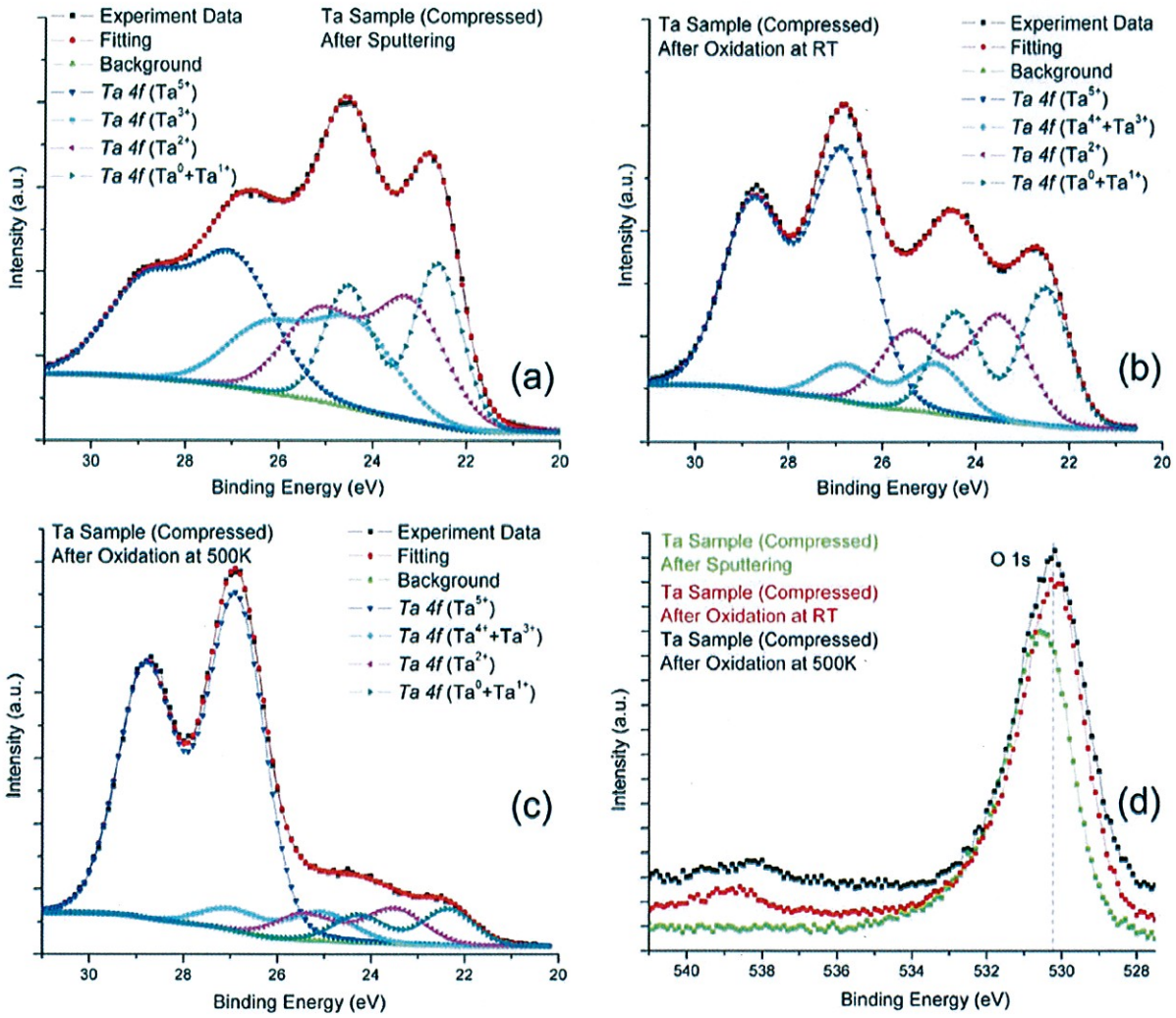

Figure 2. XPS results of compressed polycrystalline tantalum: (a) Ta 4f after sputtering; (b) Ta 4f after oxidation at RT; (c) Ta 4f after oxidation at 500 K; (d) comparison of O 1s XPS results.

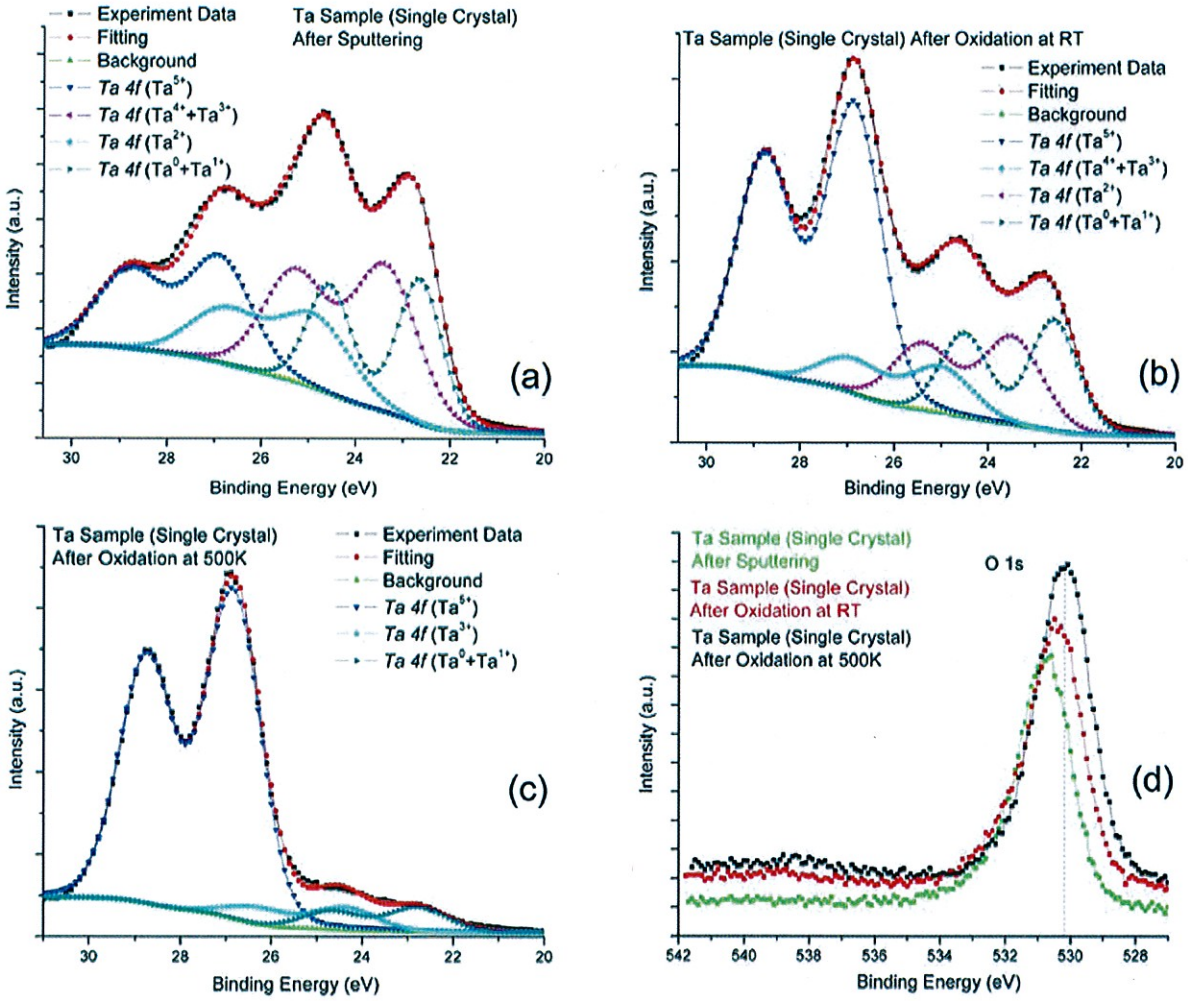

Figure 3. XPS results of single-crystalline tantalum: (a) Ta 4f after sputtering; (b) Ta 4f after oxidation at RT; (c) Ta 4f after oxidation at 500 K; (d) comparison of O 1s XPS results.

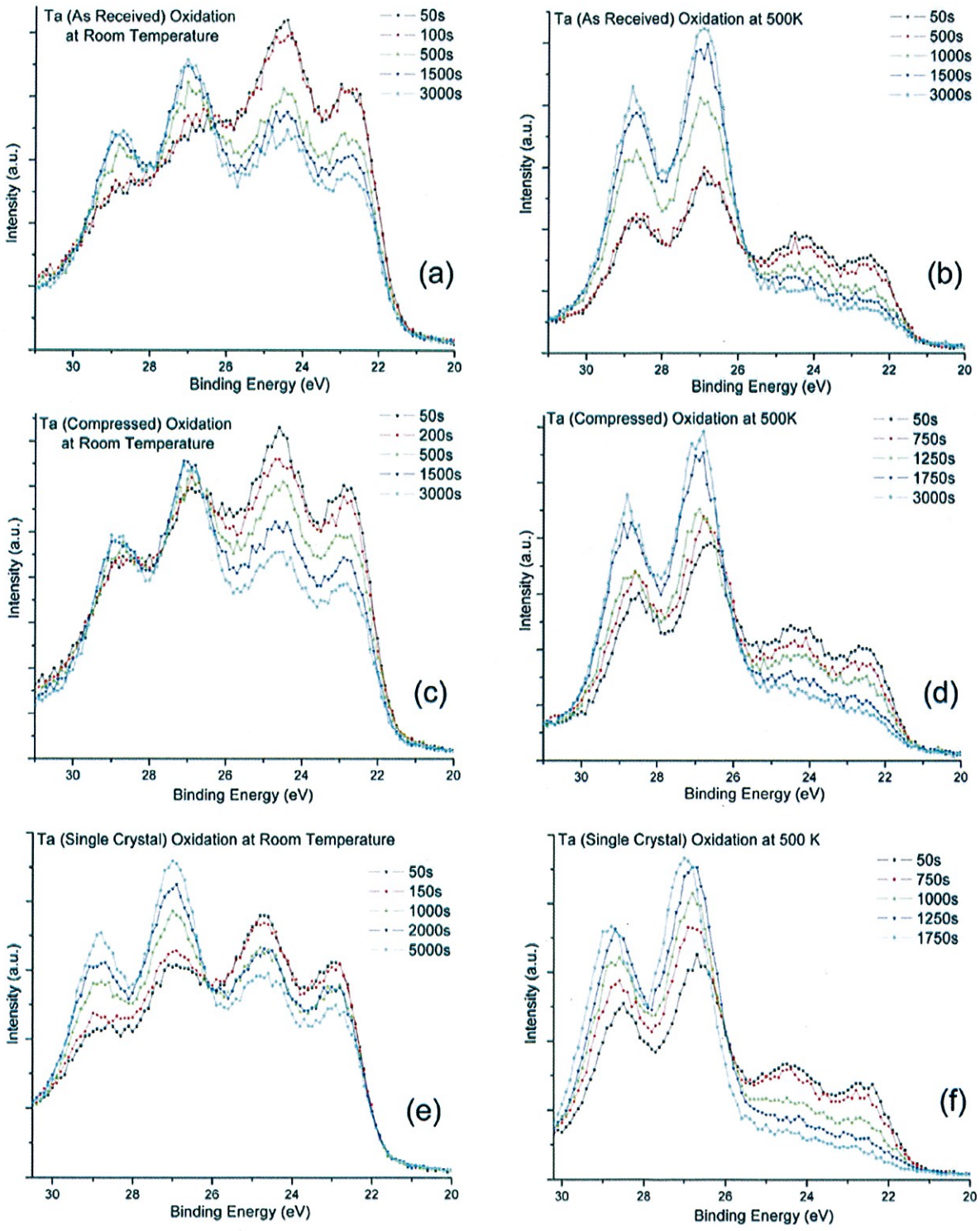

Figure 4. Time evolution of the Ta 4f region during oxidation in 0.1 Torr of O2: (a) oxidation of the as-received sample at RT; (b) oxidation of the as-received sample at 500 K; (c) oxidation of the compressed sample at RT; (d) oxidation of the compressed sample at 500 K; (e) oxidation of the single-crystal sample at RT; (f) oxidation of the single-crystal sample at 500 K.

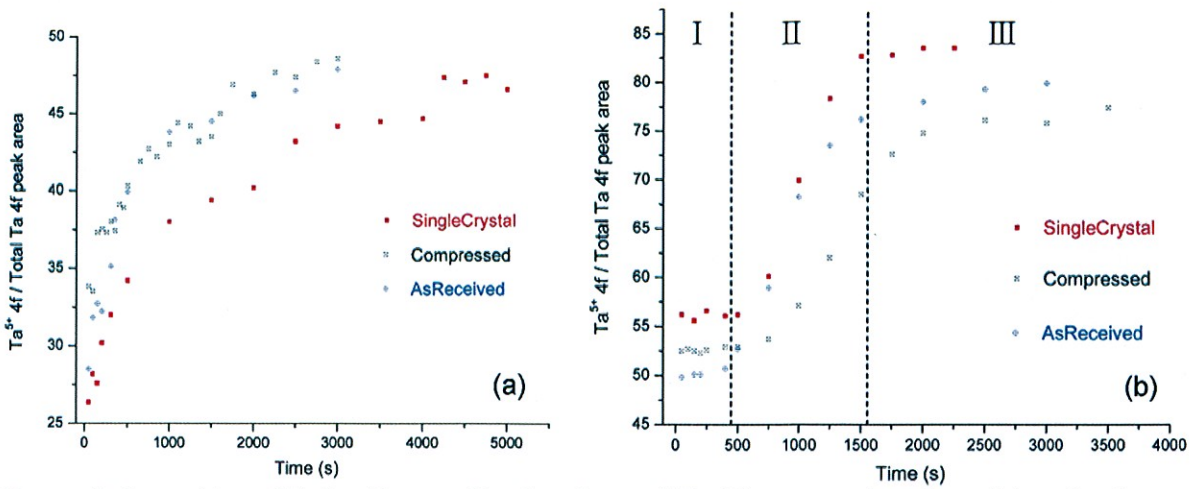

Figure 5. Intensities of Ta5+ 4f normalized to the total Ta 4f area as a function of time for three samples: (a) oxidation at RT; (b) oxidation at 500 K.

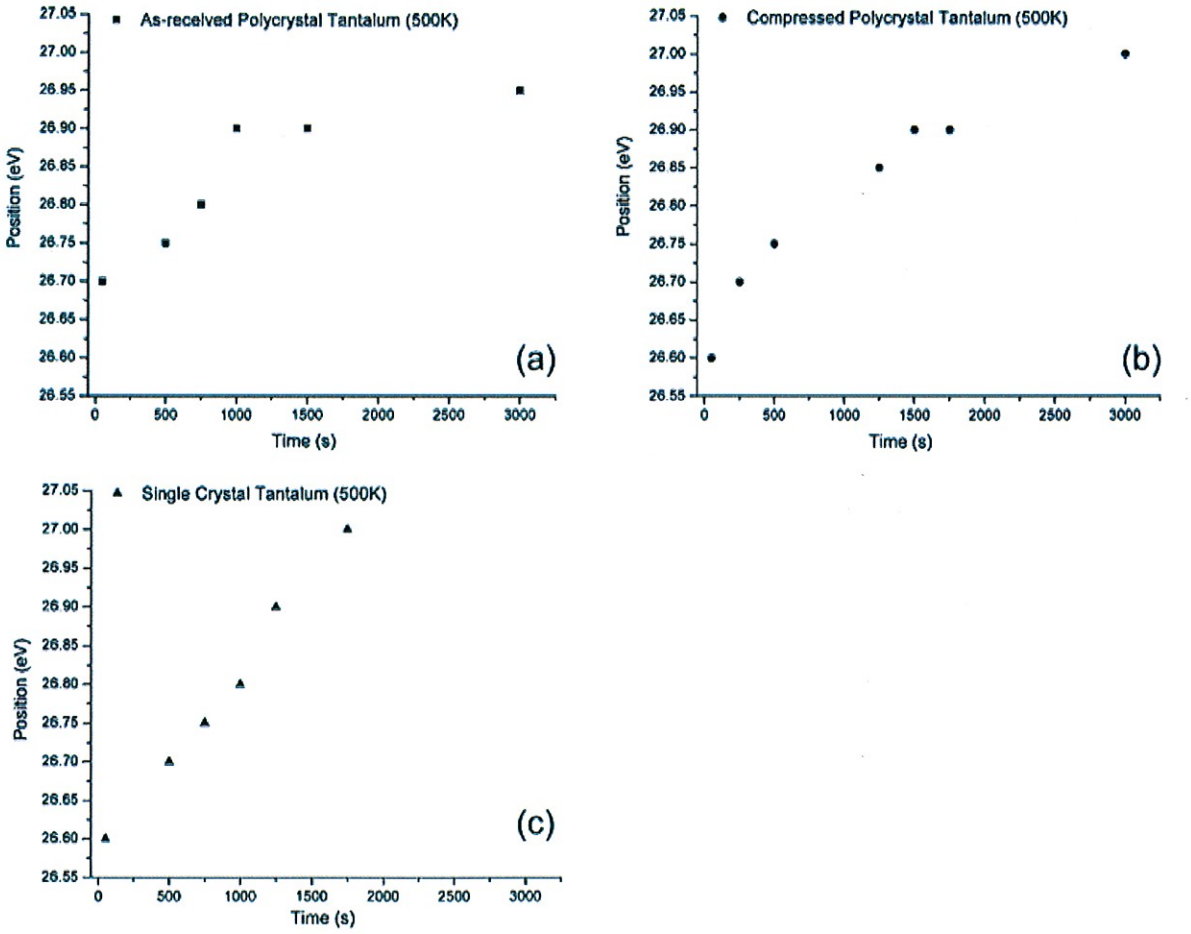

Figure 6. Peak shifts of Ta 4f7/2 during oxidation at 500 K: (a) as-received sample; (b) compressed sample; (c) single-crystal sample.

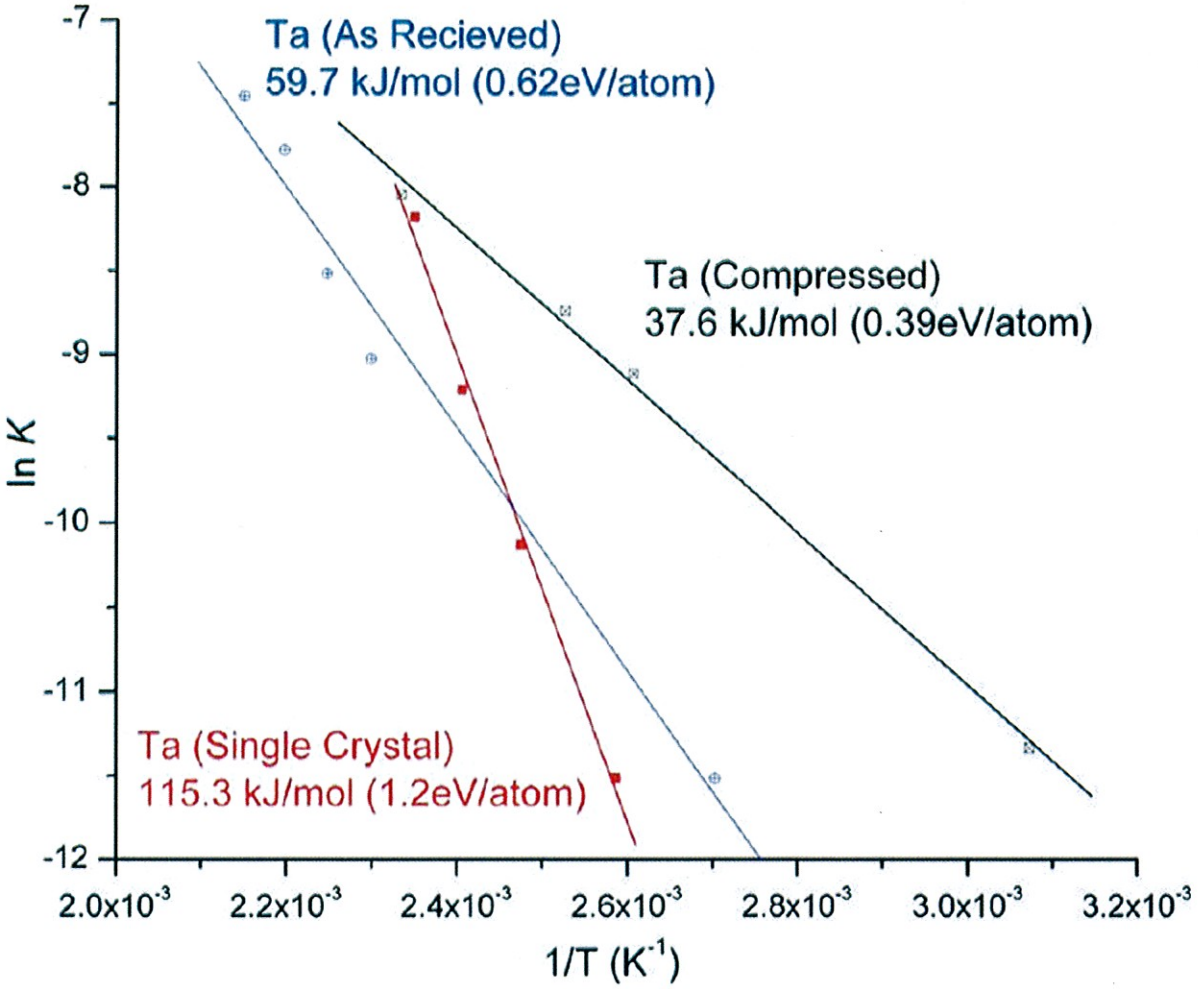

Figure 7. Activation energy calculation of three samples oxidized at 500 K.

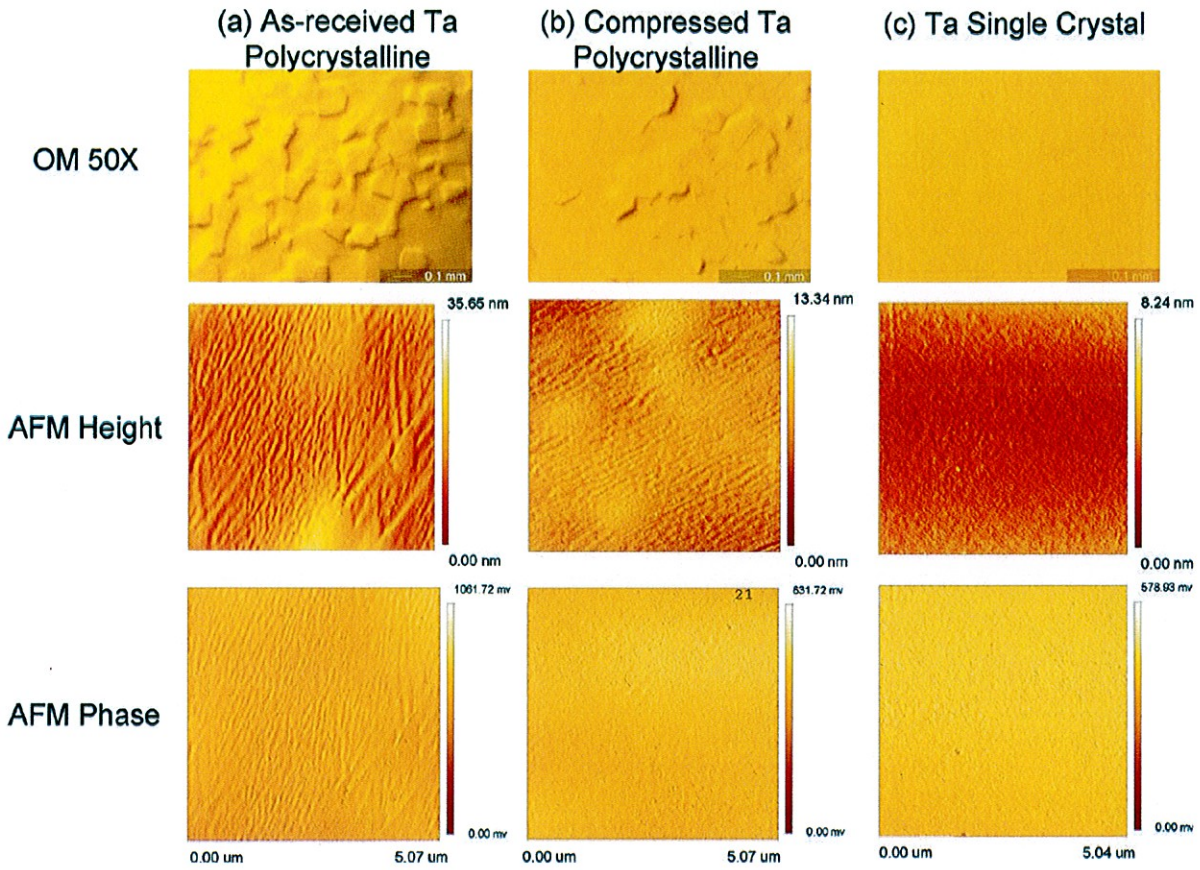

Figure 8. OM and AFM images of Ta samples: (a) as-received Ta polycrystal; (b) compressed Ta polycrystal; (c) Ta single crystal (100).

LEGAL DISCLAIMER